Continental Shelf Research 232 (2022) 104627

Contents lists available at ScienceDirect

Continental Shelf Research

journal homepage: www.elsevier.com/locate/csr

Multiscale analysis of living benthic foraminiferal heterogeneity: Ecological advances from an intertidal mudflat (Loire estuary, France)

A. Thibault de Chanvalon [a,*], E. Geslin [b], M. Mojtahid [b], I. Métais [c], V. Méléder [d], E. Metzger [b]

[a] CNRS, Universite de Pau et des Pays de l'Adour, E2S UPPA, IPREM, Pau, France
[b] Univ Angers, Université de Nantes, CNRS, LPG, F-49000 Angers, France
[c] Université Catholique de l'Ouest, BIOSSE, Angers, France
[d] Nantes Université, Institut des Substances et Organismes de la Mer, ISOMer, UR 2160, Nantes, France

A B S T R A C T

An unprecedented sampling effort on the Loire estuary allowed a multi scale approach to identify parameters controlling density variations of benthic foraminifera. Indeed, the distances between the samples analysed for this study vary from 1 cm to hundreds of kilometres. To catch this range of distance variations, a model called Scale Variance Analysis was build describing the participation of each scale to the total observed variance. The SVA model requires, for each scale, the stability of relative variance. A comparison with the Moran's Index and experimental variogram is proposed showing coherent conclusions with the SVA analysis. The analysis shows that in order to maximize information on foraminiferal density variation, sampling campaigns should be designed with stations distant from few meters to 1 km, with a particular focus on the hectometre scale. A range of scale too rarely investigated in the community of benthic foraminifera ecology. Next, based on two intertidal mudflat stations separated of few hundred meters, the present study shows that for *Ammonia tepida*, the scale dependant preponderant parameters is the Chl a concentration in the top first centimetre. Contrastingly, the indicators of food quality such as the lability index and the oxygen penetration depth do not seem to affect *A. tepida* densities. This high quantity, low quality diet is interpreted as an opportunistic behaviour that is indirectly confirmed by a kinetic approach. This approach compares the deep infaunal microhabitat density with the shallow infaunal microhabitat density. The identical ratio indicates quick saturation of the available resources.

1. Introduction

Benthic foraminifera are ubiquitous in sediment, giving them the potential to be bio-indicators of ecosystem functioning in all marine environments including transitional areas such as intertidal mudflats (*e. g.* Debenay et al., 2001; Schönfeld et al., 2012). Moreover, their distribution evolves monthly to seasonally (Alve and Murray, 2001; Kitazato et al., 2000) which fits with the frequency of most survey sampling and smooths the influence of environmental parameters that changes more rapidly (*e. g.* semi-diurnal tides). However, a comprehensive framework of their spatial heterogeneity is still lacking, while it could be an important step towards a standardization of the sampling strategy required for the optimization and generalization of their use as bio-indicators (Schönfeld et al., 2012). Additionally, assuming that a consequence has similar heterogeneity that its cause, multiscale analysis of heterogeneity would improve our understanding of the preponderant parameters controlling species distribution (*e. g.* Talley 2007).

Since the 50's, ecological studies take advantage of some mining engineer geostatistical methods to express the spatial distribution variability using synthetic indices (Legendre and Fortin, 1989). For example, the Moran's Index (Moran, 1950) has been applied on benthic foraminifera by Hohenegger et al. (1993) and Thibault de Chanvalon et al. (2015) to identify scales of patchiness. However, in the case of our study from the Loire estuary, to compare samples acquired at different spatial resolutions, and with a different sampling size, scale variance analysis is better-suited (Moellering and Tobler, 1972). In the Loire estuary, Mojtahid et al. (2016) documented the spatial distribution patterns of living foraminifera at a kilometric to decametric scale using a Van Veen grab sampler while Thibault de Chanvalon et al. (2015) described foraminiferal distribution based on 1 cm^3 samples from the intertidal mudflat "Les Brillantes". New data from 6 sites on the "Les Brillantes" mudflat distant from few metres to hundreds of metre are here gathered with the Mojtahid et al. (2016) and the Thibault de Chanvalon et al. (2015) datasets.

In the present paper, we will illustrate the role of such geostatistical tools to characterise the preponderant factor controlling some species distribution following a three steps demarche consisting in i) exploring, ii) identifying and iii) validating the causality relationship. In the case of the *Ammonia tepida* density distribution in the Loire estuary, we will i) determine the most significant scale to assess spatial foraminiferal

* Corresponding author.
E-mail address: aubin.thibault-de-chanvalon@univ-pau.fr (A. Thibault de Chanvalon).

https://doi.org/10.1016/j.csr.2021.104627
Received 6 January 2021; Received in revised form 15 November 2021; Accepted 27 November 2021
Available online 2 December 2021

density variation based on multiscale analyses, in order to ii) identify the preponderant mechanism controlling foraminifera density assuming it has a similar heterogeneity. This second step will be achieved looking at direct correlation with foraminifera density. To validate this deterministic approach we will iii) test the steady state between foraminifera density and the controlling factor based on vertical distribution analysis. Hence, with depth, different microhabitat characterised by different feeding time, exchange their population due to mobility or bioturbation. We will demonstrate that equilibrium between the density of these microhabitats indicate steady state regime at all depths.

2. Materials and methods

2.1. Study area

"Les Brillantes" mudflat is located in the inner part of the Loire River estuary (Fig. 1), the outlet of a 117,045 km^2 - drainage basin composed of both sedimentary and granitic rocks. The mean discharge of the Loire River is 900 m^3s^{-1}, varying from 120 m^3s^{-1} in summer to over 5000 m^3s^{-1} during winter flood, and leading to a high seasonal variability of water salinity at "Les Brillantes". The Loire estuary is macrotidal and hypersynchronous (Le Floch, 1961) with a tidal range from 2 to 7 m, producing large intertidal areas ("Les Brillantes" is 1350 ha) and important sediment resuspension. Therefore, sediment grain size characteristics at "Les Brillantes" is quite homogeneous with silty-clay unimodal deposits with a median size of between 10 and 20 μm (Coynel et al., 2016). The 12 h tidal cycling produces large daily changes of salinity and structuration of water column, especially when it chimes with low flow (that mostly varies seasonally, see Thibault de Chanvalon et al., 2016) and high tidal intensity (whose main cycle lasts 2 weeks). Depending on the period of the year, the moment of the lunar cycle and the time of the tidal cycle, salinity at the sampling point can vary from 35 to 0 and was about 20 in May 2013 and 14 in September 2012.

Two stations on the unvegetated slikke were chosen to study the spatial variability at the metre scale in "Les Brillantes" mudflat (Fig. 1): Site 1 is located 20 m offshore from a 1 m-high-eroded cliff while Site 2 is 500 m offshore. The main difference between the two stations lies in the longer emersion time for site 1, the closest to the shore. According to Benyoucef (2014), Site 1 is characterized by a denser microbiofilm (*i.e.* microphytobenthos composed of diatoms).

2.2. Sampling strategies

In this study, the estimation of metric heterogeneity for micro and meiofaunal (*i.e.* foraminifera) composition is based on three replicate interface cores (triplicates cores) from the same site, distant from each other by few meters. For all the other measured parameters (oxygen profiles, macrofauna), a dedicated core was sampled from each site. A similar vertical sampling resolution was used for all analyses *i. e.* cores with inner diameter of 8.2 cm, were sliced every 2 mm until 2 cm and every 5 mm until 5 cm with the exception of macrofauna of which the abundance was determined for the full core depth. To minimise the temporal variability, the foraminifera samples were acquired in September 2012 and May 2013, simultaneously to those from Mojtahid et al. (2016, sampled in September 2012) and Thibault de Chanvalon et al. (2016).

2.3. Biological compartment

The core triplicate dedicated to foraminifera was sliced few hours after recovery and incubated overnight in Cell-Tracker™ Green (Invitrogen Detection Technologies)/dimethylsulfoxide (DMSO) mixture (final concentration of 1 μmol L^{-1}) then preserved in 10% formaldehide/3.8% borate mixture. This method was chosen for its accuracy at discriminating living from dead foraminifera since it reacts with enzymes to produce a fluorescent compound (see details in Bernhard et al., 2006). Only the larger (>150 μm) fraction including adult specimens was conserved for identification (see detailed procedure in Langlet et al., 2014). Then, only foraminifera fluorescing continuously and brightly under an epifluorescent binocular (Olympus SZX12 with a fluorescent light source Olympus URFL-T) were picked out, counted and determined. Note that, the species that we refer to as *Ammonia tepida* in the following text corresponds to the phylotype T6 according to the recent classification of *Ammonia* sp. (Richirt et al., 2019). This is a common *Ammonia* phylotype in the European intertidal mudflats (Bird et al., 2020).

Foraminiferal oxygen uptake (FOU) is calculated with equation (1), with $R_i(T_{13})$ being the respiration rate of the species i from laboratory measurement at 13 °C in pmol O_2 ind^{-1} d^{-1} from Geslin et al. (2011), the exponential being the Arrhenius temperature correction (with T_A a constant in °C determined by Bradshaw, 1961) and d^o_i the measured

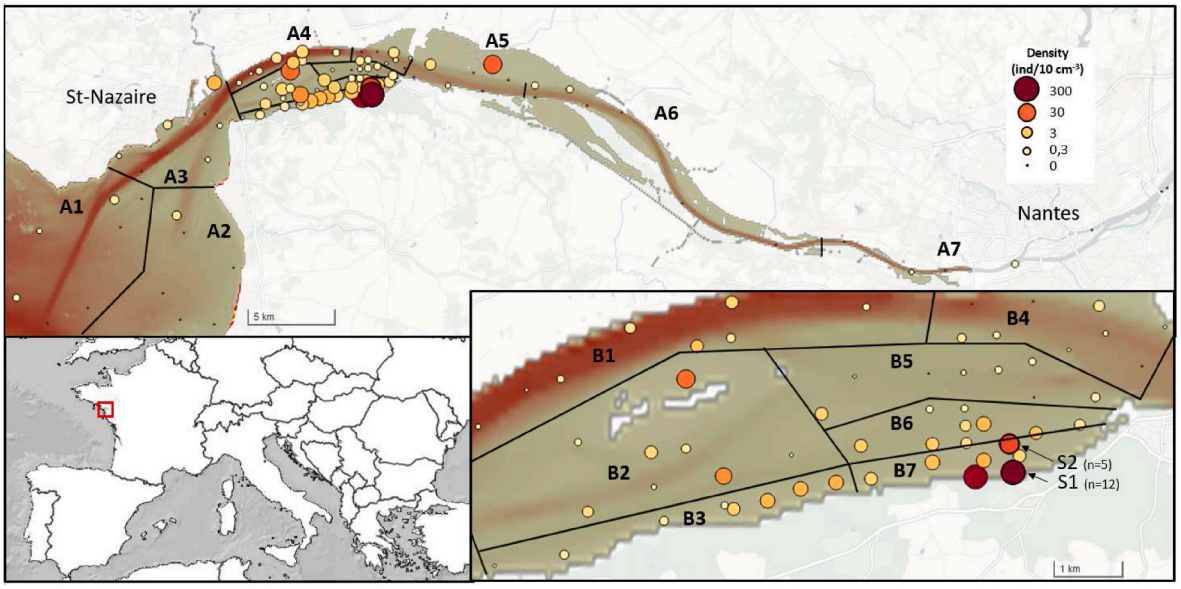

Fig. 1. Bathymetry of the Loire estuary with surface density of *A. tepida* from Mojtahid et al. (2016) sampled in September 2012, Thibault de Chanvalon et al. (2015) sampled in May 2013 and this study (both May 2013 and September 2012). Black lines indicate regions used in the scale variance analysis for the scale 7 (A1 to A7) and the scale 6 (B1 to B7). Bottom right insert focus on the "Les Brillantes" mudflat (Map produced on R using leaflet package, bathymetry from the SHOM).

areal density of living foraminifera in the oxic layer in ind m^{-2}:

$$FOU = \sum_i R_i(T_{13}) \exp\left(\frac{T_A}{T_{13}} - \frac{T_A}{T_{obs}}\right) \; d_i^O \quad (1)$$

We calculated the average living depth ALD_x, initially proposed by Jorissen et al. (1995) to describe quantitatively the microhabitats distribution, following equation (2):

$$ALD_x = \frac{\sum_i n_i D_i}{\sum_i n_i} \quad (2)$$

With n_i the number of specimens in interval i, D_i the midpoint of sample interval and x the lower boundary of the deepest sample.

Another core triplicate was dedicated to microphytobenthos (MPB) and frozen *in situ* by liquid nitrogen. Pigments extraction used a cold mixture (4 °C) of 90% methanol/0.2 M ammonium acetate and 10% ethyl acetate (90/10 vol/vol) and measurement performed by HPLC (see Méléder et al., 2005 for details). To assess organic matter quality, we used the lability index, LI = Chl *a*/(Chl *a* + Pheo *a*), with Pheo *a* corresponding to the total amount of phaeophorbides a and pheophytins a, respectively due to grazing and microbial activity (*e.g.* Bianchi and Findlay, 1991; Cartaxana et al., 2003).

Finally, each core of the triplicate dedicated to the macroinvertebrates was homogenized over its full depth (35 cm) sieved at 1 mm and preserved in 4% formaldehyde before species identification and counting in the >1 mm fraction.

2.4. Oxygen fluxes

Dissolved oxygen vertical profiles were measured in a separate core in the dark, within few hours after sampling using a Clark-type microelectrode with a 50 μm thick tip (OX50, Unisense, Denmark) connected to a multimeter (Unisense) in a temperature controlled bath. Twelve and 10 oxygen profiles were measured in September 2012 and 24 and 4 profiles in May 2013 at stations S1 and S2 respectively. Diffusive O_2 uptake (DOU) was estimated with the PROFILE software by fitting the measured oxygen concentration with concentration from diffusion-reaction models (see details in Berg et al., 1998).

2.5. Statistical analysis

2.5.1. Moran's index

Patchiness effect was explored using spatial correlograms built using the Moran's Index (I), computed with R (package "spdep" following Bivand and Wong, 2018 and Fortin and Dale, 2005, Equation (3)). This index calculates the similarity of pair values for one neighbourhood compared to the global mean of the dataset, a neighbourhood being defined by a weighted (w_d) function of the distance (l_{ij}) between the pair values (x_i, x_j). Here, we used a weighted function sensitive only to the scale of the distance, *i. e.*:

$$I(d) = \frac{\sum_i^n \sum_{j\neq i}^n W_d(I_{ij})(X_i - \overline{X})(X_j - \overline{X})}{\sum_i^n (X_i - \overline{X})^2} \times \frac{n_d}{\sum_i^n W_d(I_{ij})} \quad (3)$$

with

$$w_d(l_{ij}) = \begin{cases} 1, \; 10^d < l_{ij} < 10^{d+1} \\ 0, \; otherwise \end{cases} \quad (4)$$

and d, the scale of interest, n, the number of samples and n_d the number of samples forming at least one pair. Significance of values is estimated based on Monte-Carlo analyses provided in the "spdep" package (function moran.mc, done with 9999 simulations). This function compares the I value obtained from the original dataset with a distribution produced by many simulated I values. First, these simulated I values were obtained by random distribution of all density values. Second, to take into account that in some case, very few sample formed pairs, the simulated I values were obtained by exchanging randomly 10% of the samples forming pairs with random samples from the dataset.

2.5.2. Scale variance analysis

Scale variance analysis (SVA) decomposes the total variance of a dataset to identify the contribution of each scale to the variance (Moellering and Tobler, 1972; Wu et al., 2000). The SVA compares each sample to a local mean which complements the Moran's Index, in which samples are compared to the global mean. This approach requires *a priori* explicit definition of scales of interest and *a priori* delimitation of all regions, necessarily nested over the different scales. By convention, for a dataset hierarchized over k scales of interest, the scale 1 is the size of the initial samples, that are gathered in local regions belonging to the scale 2. Then, the mean of each local regions is treated as sample of the scale 2 and are gathered again in intermediate regions belonging to the scale 3. The process is repeated until the scale k, covering the extent over which the sampling has been done. On each scale, the concept of "scale variances" is introduced which corresponds to the variance of samples of scale h over a region of scale h+1.

The following details are inspired from Moellering and Tobler (1972) but using different writing. For samples of the scale h, gathered in regions belonging to the scale h+1, the scale variance, $V_i^{h\to h+1}$, is defined according to equation (5).

$$V_i^{h\to h+1} = \frac{1}{n^h} \sum_{j=1}^{n^h} \left(x_i^{h+1} - x_{i,j}^h\right)^2 \quad (5)$$

With x_i^{h+1}, the mean value of all samples nested in the group i; $x_{i,j}^h$ the different sample (whose size is belonging to the scale h) value constituting the group i and n^h the number of sample $x_{i,j}^h$ constituent the group i. For simplicity, we here assume that n^h does not depend of i, *i.e.* all groups of size belonging to the scale h+1, are constituted by the same number of sample from the scale h. Then, for being representative of the importance of the variance of a certain scale (h) over the whole dataset one need to look at the mean of the scale variances of the scale h, according to equations (6) and (7)

$$\overline{V^{h\to h+1}} = \frac{1}{N^{h+1}} \sum_{i=1}^{N^{h+1}} V_i^{h\to h+1} \quad (6)$$

with

$$N^{h+1} = \prod_{p=h+1}^{k} n^p \quad (7)$$

Equation (7) describes that N^{h+1} is equal to the number of group whose size belonging to the scale h+1. Thus, one can demonstrate (see Appendice 1) that for a dataset hierarchized over k scale of interest, the variance (VAR) can be decomposed into the sum of the mean of the scale variances (equation (8)):

$$VAR = V^{1\to k} = \sum_{h=1}^{k-1} \overline{V^{h\to h+1}} \quad (8)$$

However, SVA requires a complete dataset with all values of scale 1 totally enumerated (Moellering and Tobler, 1972). In our case, the data range over 8 orders of magnitude from samples at the cm scale to a sampling area of hundreds of kilometres. Assuming 5 samples per group, an exhaustive sampling would require $5^7 = 78.125$ analyses. To overcome the analytical limitation to produce so many analyses, a supplementary assumption is required: the scale stability of relative variance. For each scale, this assumption assumes that all groups i are characterized by the same relative scale variance ($RV^{h->h+1}$). The $RV^{h->h+1}$ is defined as the square of the relative standard deviation *i. e.* for any i:

$$RV^{h\to h+1} = \frac{V_i^{h\to h+1}}{\left(x_i^{h+1}\right)^2} \quad (9)$$

This is a heavy assumption but it allows the calculation of any mean scale variance as soon as both the relative scale variance and the sum of the square of the mean of all higher scale are known (see Appendice 2) according to equation (10):

For any h ≤ k-2

$$\overline{V^{h\to h+1}} = \frac{RV^{h\to h+1}}{N^k}\prod_{i=h+1}^{k-1}\left(1+RV^{i\to i+1}\right)\sum_{j=1}^{N^k}\left(x_j^k\right)^2 \quad (10)$$

This relation indicates that the means of the scale variances for a certain scale can be calculated as soon as the relative scale variance is known. Lastly, this relation indicates that direct comparison of the relative scale variance from different scales of the same dataset is not meaningful and that comparison of the mean scale variance has to be preferred.

2.5.3. Experimental variogram

To complement Moran's Index, that compares samples to the global mean, and SVA, that compares samples to a local mean, an experimental variogram was built. In this case, each pair of samples is compared to the square of their difference without referring to any external mean. Then, the gamma value (γ) is computed as the half of the mean of the values that belong to a certain distance, according to equation (11).

$$\gamma(d) = \sum_i^n\sum_{j\neq 1}^n W_d\left(I_{ij}\right)\left(X_i - X_j\right)^2 \times \frac{1}{2\sum_{i,j}^n W_d\left(I_{ij}\right)} \quad (11)$$

with

$$w_d\left(l_{ij}\right) = \begin{cases} 1, & 10^d < l_{ij} < 10^{d+1} \\ 0, & otherwise \end{cases}$$

2.5.4. Application to the Loire estuary dataset

Moran's index, SVA and experimental variogramare calculated based on the average density of *A. tepida* in the first centimetre depth measured in this study, in Thibault de Chanvalon et al. (2015) and in the study of Mojtahid et al. (2016). This combined dataset is represented in Fig. 1 and is not regularly distributed in the Loire area. For example, for the Moran's index calculation, each class of distance covering scales from centimetre to hectometre (hundreds of meters) are represented by less than 72 sample pairs. The scale variance analysis (SVA) was calculated based on regions delimited arbitrary by the black lines on Fig. 1. The column "available sampling/exhaustive sampling" in Table 1 summarized the number of regions per scale and compared it with an exhaustive sampling as theoretically requested. The scale levels 3, 4 and 5 does not contain enough samples to be gathered into at least one group. Thus, the mean of the scale variance for scale 3, 4 and 5 could not be calculated directly and was estimated by the difference between the global calculated variance and all the means of the scale variance. Moreover, all information for close (<100 m) samples belong to or are close to stations 1 and 2. Nevertheless, such limitations are very frequent in foraminiferal dataset and the spatial recovery obtained with this combined dataset is rare in the literature motivating the pursuit of the spatial heterogeneity analysis.

2.6. Model of microhabitat equilibrium

The relation between deep infaunal and shallow infaunal foraminiferal faunas is modelled using a dynamic 2 boxes-model (whose equations are detailed in Fig. 2A) based on typical assumptions drawn from ecological studies (Levin, 1976). The shallow infaunal box is characterised by a population (pop_{sh}), a first order mortality rate (k_{d_sh}) and a reproduction rate described with the Verhulst equation, that is, a first order rate (k_p) decreasing to zero as the population saturates (pop_{sat}) available resources. The deep infaunal box is characterised by a population (pop_{de}) and a first order mortality rate (k_{d_de}). The transfer between the 2 boxes follows a first order rate (k_{ech}), roughly estimating biomixing. The ratio of deep over shallow infaunal population, $\alpha = pop_{de}/pop_{sh}$, predicted by this model after an important increase of environment capability (by 500 fold in this example) is shown in Fig. 2B. First the shallow population increase, hence α decrease. After a short delay, deep infaunal population increase too, leading to an equilibrium between exponentially growing shallow and deep infaunal population and α reaching a plateau (α_{exp}, on Fig. 2B). The higher k_{ech} is, the faster the first plateau is reached. Finally, once the population reaches the limits of the environment capabilities another equilibrium is observed between the two populations that is characterised by a second plateau (α_{sat} on Fig. 2B). The higher k_p is, the faster the second plateau is reached, other parameters having much less influence on the rate of α changes. The α value at the plateau is defined as:

$$\alpha_{sat} = \frac{k_{ech}}{k_{ech} + k_{d\_de}} \quad (12)$$

$$\alpha_{exp} = \begin{cases} 1 - \frac{b}{2} & if\ b \ll 2 \\ \frac{1}{b} & if\ b \gg 2 \end{cases}$$

with

$$b = \frac{k_p + k_{d\_de} - k_{d\_sh}}{k_{ech}}$$

3. Results

3.1. Environmental parameters

Table 2 summarizes most of the environmental parameters extracted from public survey databases (banque HYDRO, SYVEL and SHOM networks, see glossary) and previous publications (Benyoucef, 2014; Thibault de Chanvalon et al., 2016).

The two campaigns were characterized by contrasted river discharge (150 $m^3\ s^{-1}$ in September versus 1200 $m^3\ s^{-1}$ in May), organic carbon

Table 1
Scale variance analysis.

Scale level (h)	Characteristic scale distances (10^{h-3} m)	Family size* (n^h)	Available sampling/ exhaustive sampling	Relative scale variance ($RV^{h\to h+1}$)	$\frac{1}{N^h}\sum_{i=1}^{N^h}(x_i^h)^2$	Mean of the scale variance ($\overline{V^{h\to h+1}}$)	$\frac{\overline{V^{h\to h+1}}}{VAR}$ x 100	$\frac{\overline{V^{h\to h+1}}}{VAR}$ x 100†
8	100 km		1/1		5.904			
7	10 km	7	7/7	2.318		14.38	0.9	0.6
6	1 km	7	7/49	3.513		74.19	4.6	2.5
5	100 m	7	0/343				*26.6*	*28.2*
4	10 m	7	0/2401				*26.6*	*28.2*
3	1 m	7	2/16 807				*26.6*	*28.2*
2	1 dm	5	106/84 035	0.083		114.85	7.1	4.6
1	1 cm	7	7/588 245	0.083		125.54	7.7	7.7

* Number of samples of order h required to constitute a sample of order h+1, † calculated after exclusion of S1 from the dataset.

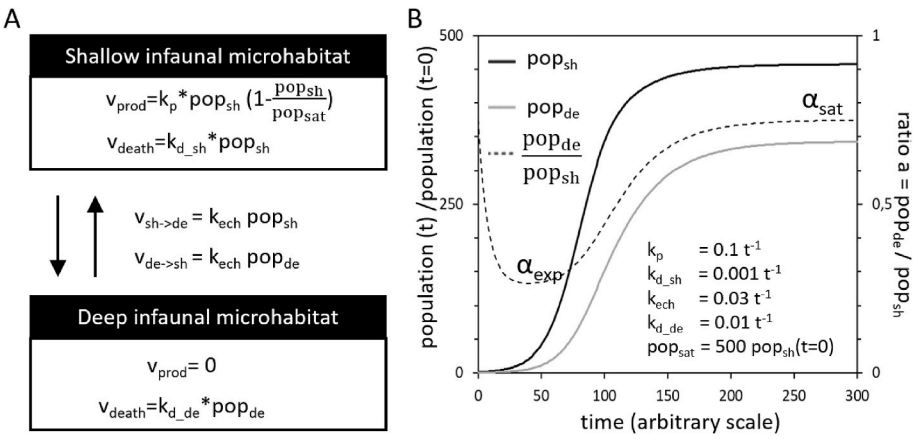

Fig. 2. A. Deterministic model to explain these relations based on biomixing and chemotaxis forcing. v_{prod}, v_{death}, $v_{sh-\ >\ de}$ and $v_{de-\ >\ sh}$ correspond to the rate of reproduction, the rate of death, the rate of exchange from shallow to deep microhabitat and the rate of exchange from deep to shallow microhabitat respectively. k_p, k_{d_sh}, k_{d_de} and k_{ech} are the associated parameters while pop_{sh} and pop_{de} are the population of shallow and deep microhabitat. B. Example of a representative result from the model following a 500 fold increase of environment capability, *i. e.* 500 fold pop_{sat} increase.

Table 2
Geochemical parameters.

		Sept 2012	May 2013
	Average flow (m^3s^{-1})	150	1200
	Salinity[a]	22 ± 5	8 ± 7
	Water Temperature (°C)[a]	17 ± 0.5	13 ± 1
	Tidal coefficient[b]	50 ± 10	80 ± 20
S1	Grain size nomination[c] (0–5 cm)	silty clay	silty clay
	Oxygen Penetration Depth (mm) (±SD)	2.3 (±0.4, n = 12)	1.9 (±0.2, n = 24)
	Dissolved phosphorus in 0–1 cm[5] (µmol L^{-1})	15.4	14.2
	Total Organic Carbone in 0–1 cm[5] (%)	2.3	2.8
S2	Grain size nomination[c] (0–5 cm)	silty clay	silty clay
	Oxygen Penetration Depth (mm) (±SD)	4.7 (±0.7, n = 10)*	1.4 (±0.2, n = 4)
	Dissolved phosphorus in 0–1 cm[5] (µmol L^{-1})	2.7	4.8
	Total Organic Carbone in 0–1 cm[5] (%)	2.1	2.8

*Most of the profiles show bioturbation.
[1] measured at Mont-Jean sur Loire (banque HYDRO).
[5] from Thibault de Chanvalon et al. (2016)
[a] GIP Loire.
[b] SHOM.
[c] From Benyoucef (2014).

content in the top of sediment (2.1% versus 2.8%), salinity (22 versus 8, respectively) and temperature (17 °C versus 13 °C). Contrastingly, nutrients showed mainly spatial variation with a higher concentration of dissolved phosphorus at Station 1, closer to the shore, with 15.4 and 14.2 µmol L^{-1} for September 2012 and May 2013 respectively, compared to 2.7 and 4.8 µmol L^{-1} for Station 2 (Thibault de Chanvalon et al., 2016). Finally, the oxygen penetration showed both important spatial and temporal variability with a lower value in May 2013.

3.2. Biological parameters

Table 3 indicates that the three studied biological compartments differ significantly between the two stations and less clearly between the two campaigns. Station 1 shows higher abundances of microphytobenthos (the average of the two campaign for chlorophyll A is 340 mg m^{-2} in Station 1 versus 180 mg m^{-2} in Station 2), macrofauna (770 ind m^{-2} in Station 1 versus 290 ind m^{-2} in Station 2 on average) and living foraminifera (78 ind/10 cm^3 versus 24 ind/10 cm^3) than Station 2. While *Ammonia tepida* (>70%) dominates foraminiferal communities in both stations, macrofaunal assemblages switch from a dominance of the polychaetes *Hediste diversicolor* (>75%) at Station 1 to a dominance of both the bivalve *Scrobicularia plana* and the polychaetes *Heteromastus filiformis* at Station 2. The main seasonal variation visible in both stations is for macrofauna with an increase of *H. filiformis* associated to a decrease of *S. plana* in May 2013. However, in Station 1, but only there, foraminifer density decreases significantly in May 2013 with, for example, a near disappearance of *H. germanica* going from 36 ind/10 cm^3 down to 2 ind/10 cm^3 in the first top centimetre. The lability index (LI), that is higher than 0.9 in both stations and seasons, indicates important *in situ* autotrophic activity of microphytobenthos.

3.3. Vertical distribution

The densities of benthic foraminifera and Chl a concentration presented in Fig. 3 show in several cases an exponential decrease of densities with depth. The high density of *H. germanica* in the top 2 mm in September 2012 at Station 1 (67 ind/10 cm^3) appears concomitantly to particularly high densities of *A. tepida* (829 ind/10 cm^3) and Chl a (201 mg m^{-2}). However, in detail, the exponential decrease associated to this high density appears more progressive than for *A. tepida* and Chl a, with a minimum reached at 1.4 mm depth for *H. germanica* versus 0.6 mm depth for the others.

3.4. Foraminifera aerobic respiration rates

The respiration rates (RR) estimated for the foraminiferal population for each season and station as well as the relative foraminiferal contribution to DOU are shown in Table 4. The estimated respiration rates are 3357 ± 117 pmol O_2.ind^{-1}.d^{-1} and 2154 ± 75 pmol O_2.ind^{-1}.d^{-1} for *A. tepida* and 685 ± 134 pmol O_2.ind^{-1}.d^{-1} and 439 ± 86 pmol O_2.ind^{-1}.d^{-1} for *H. germanica* at respectively 17 °C (September) and 13 °C (May). The maximal relative contribution of the foraminiferal fauna to DOU was 2.3%, at station S1 in September 2012 mostly carried by the dense population of *A. tepida*. For all other samplings, foraminiferal respiration rates (sum of *A. tepida* and *H. germanica* respiration rates) are much lower and varies from 0.085 to 0.099 mmol O_2 m^{-2} d^{-1}.

3.5. Statistical analysis

Fig. 4A shows that the Moran's index is significantly higher than zero for all scales below 0.1 km, which indicates that foraminiferal densities are grouped into patches of hundreds of metre's size. The negative value for Moran's index between 1 and 10 km (Fig. 4A) indicates that most of the difference between environments occurs between 1 and 10 km for *A. tepida* densities. SVA results presented in Fig. 4B (black dots) show that most of the variance (average scale variance >10%) comes from the scales between 1 m and 1 km but the lack of data (see Table 1) prevents us from a better accuracy. Interestingly, scale variance analysis quantifies that scales between 1 cm and 1 m counting for 3.6 times less to the overall variance than the scales between 1 m and 1 km. Stability of SVA, even based on our sparse dataset, is illustrated by the white dots of

Table 3
Biological parameters.

			Sept 2012			May 2013		
			Mean	SD	n	Mean	SD	n
S1	Microphytobenthos (mg m^{-2})	Chl a from 0 to 1 cm (mg.m^{-2})	384	121	3	295	185	3
		Lability Index from 0 to 1 cm	0.969	0.007	3	0.973	0.007	3
	Marofaunal density (ind m^{-2})	*Hediste diversicolor*	635		1	631		1
		Heteromastus filiformis	16		1	25		1
		Scrobicularia plana	159		1	70		1
	Foraminiferal density (ind./10 cm^{-3})	*A. tepida* from 0 to 1 cm	245	3	2	123	21	2
		A. tepida from 1 to 5 cm	53	7	2	31	8	2
		H. germanica from 0 to 1 cm	36	2	2	2	1	2
		H. germanica from 1 to 5 cm	6		1	4	1	2
	Foraminifera ALD_5 (cm)	*A. tepida*	1.54	0.17	2	1.74	0.03	2
		H. germanica	1.66		1	3.45	0.06	2
S2	Microphytobenthos (mg m^{-2})	Chl a from 0 to 1 cm (mg.m^{-2})	166	25	3	198	22	3
		Lability Index from 0 to 1 cm	0.945	0.008	3	0.978	0.011	3
	Marofaunal density (ind m^{-2})	*Hediste diversicolor*	25		1	51		1
		Heteromastus filiformis	83		1	159		1
		Scrobicularia plana	162		1	108		1
	Foraminiferal density (ind/10 cm^{-3})	*A. tepida* from 0 to 1 cm	46	12	3	60	12	2
		A. tepida from 1 to 5 cm	11	1	3	10		1
		H. germanica from 0 to 1 cm	5	1	3	5	1	2
		H. germanica from 1 to 5 cm	4	1	3	5		1
	Foraminifera ALD_5 (cm)	*A. tepida*	1.80	0.27	3	1.50		1
		H. germanica	2.76	0.21	3	2.67		1

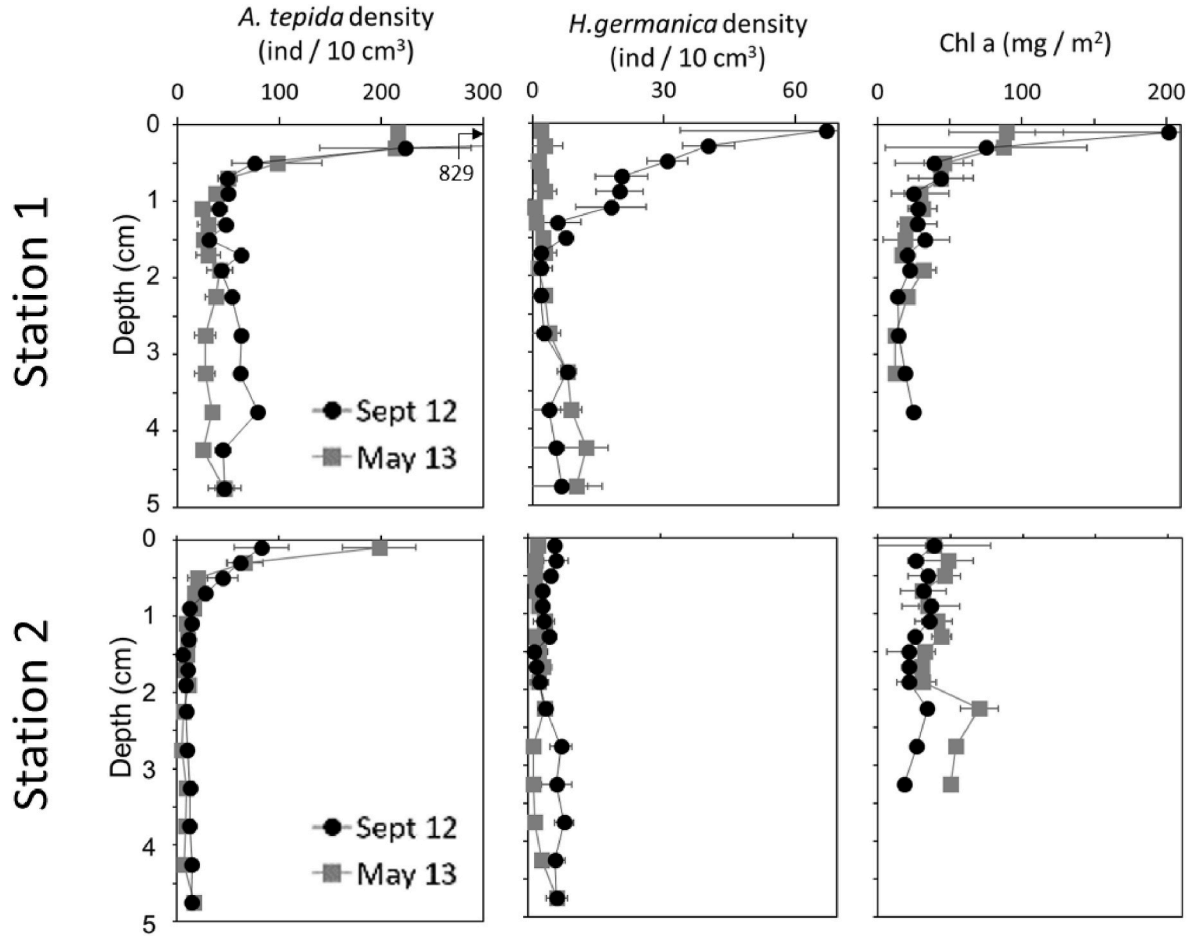

Fig. 3. Vertical distribution in the sediment column of living benthic foraminifera and Chlorophyll *a*.

Fig. 4B. It shows that the SVA processed without the particularly dense Station 1 does not modify significantly the results. Fig. 4C shows the square differences of paired samples in grey dots. The variogram calculated for each distance range is particularly high between 100 m and 1 km.

4. Discussion

4.1. Critical scale of heterogeneity identified by multiscale analysis

In "Les Brillantes" mudflat, our data show an overall high surface

Table 4
Respiration rate calculation.

Sampling date	Station	Species	Total number of foraminifera in the oxic zone (ind. 50 cm^{-2})			DOU ($mmolO_2$ m^{-2} d^{-1})			RR by foraminiferal population ($mmolO_2$ m^{-2} d^{-1})			Foraminiferal contribution to DOU %	
			Mean	SD	n	mean	SD	n	mean	SD	n	mean	SD
September 2012	S1	*Ammonia tepida*	1053	77	2	24	10.9	12	0.557	0.152	2	2.3	0.6
		H. germanica	108	28	2	24	10.9	12	0.009	0.005	2	0	0
	S2	*Ammonia tepida*	144	38	3	9.1	4.5	10	0.097	0.025	3	1.1	0.3
		H. germanica	12	4	3	9.1	4.5	10	0.002	0	3	0	0
May 2013	S1	*Ammonia tepida*	217	1	2	71	31	7	0.093	0	2	0.1	0
		H. germanica	2	1	2	71	31	7	0	0	2	0	0
	S2	*Ammonia tepida*	198	36	3	56	15	3	0.085	0.015	3	0.2	0
		H. germanica	2	1	3	56	15	3	0	0	3	0	0

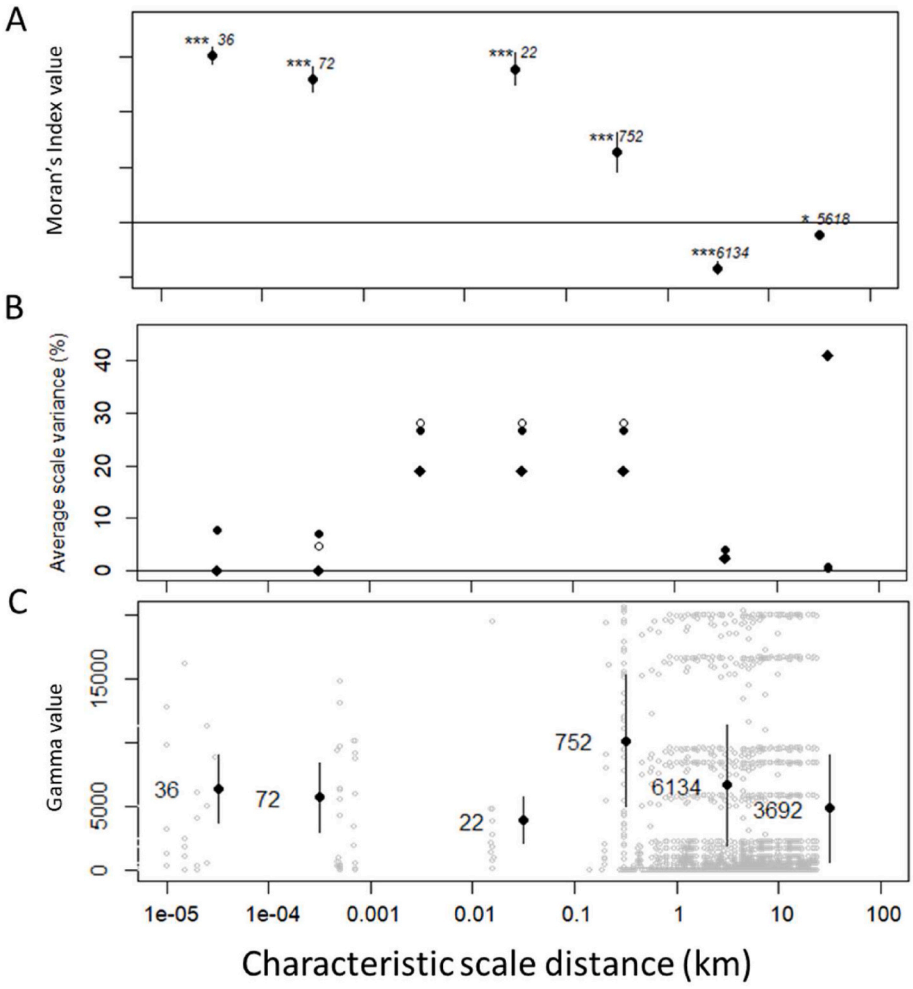

Fig. 4. Geostatistical model processes with the dataset from Fig. 1 (black dots).
Error bars in Figure A corresponds to twice the standard deviation of the distribution obtained when the samples are randomly distributed (number of simulation is 104; star attribution is based on p-value; ≤0.01***; ≤0.05**; ≤0.1*). InFigure B open circle represents the scale variance analysis (SVA) after exclusion of S1 from the dataset (open circle) and using qualitatively transformed dataset (black diamonds, see text for details). In the experimental variogram (Figure C), grey dots correspond to the square of the difference of each possible pairs, plotted against their distance. The black dots correspond to the mean and the error bars to a third of the standard deviation for each scale of distance between samples.

foraminiferal density (up to 829 ind./10 cm^3) and very low diversity (only two different species identified) (Fig. 3). High surface density (over 100 ind./10 cm^3) of foraminiferal fauna is commonly reported in intertidal mudflat surfaces from estuaries (Debenay et al., 2006; Thibault de Chanvalon et al., 2015) or inlets (Alve and Murray, 1994; Cesbron et al., 2016; Goldstein et al., 1995) while a very low diversity is more typical of macrotidal estuaries. Indeed, only the species that are the most tolerant to large daily salinity variations can grow in macrotidal estuaries (Murray, 2006), especially on non-vegetated mud. These later are for instance known for their absence of agglutinated species (Berkeley et al., 2008).

Debenay and Guillou (2002) demonstrated that the estuarine compatible species colonize successive areas along the salinity gradient. However, they did not identify the preponderant forcing among all the parameters covarying with salinity. For example, in the Loire estuary, the regular dredging of the navigation channel has also been invoked to explain the extreme poverty of the diversity of the foraminifera fauna with only three living species reported over the whole salinity gradient (Mojtahid et al., 2016). In addition to the constrains specific to estuarine environments, more common forcing such as grain size, food availability or food quality would also modify foraminiferal growth opportunities and produce, *in fine*, an irregular surface density distribution such as that illustrated in Fig. 1. In an attempt to catch such a variability, deterministic models (*e.g.* TROX model from Jorissen et al., 1995) build on predefined forcing, estimate compliance between a species and an environment while they hardly quantify the density variations. This

issue is particularly critical in dynamic environments where kinetic effects, such as new colony settling (Alve, 1999; Weinmann and Goldstein, 2017) may induce changes in hydrodynamic dispersal or hysteresis associated to transient environmental changes, prevail over saturation of the environment capabilities. A complementary approach used in ecological survey, based on geostatistical models (*e.g.* Talley, 2007) proposes at first, to synthetize spatial patterns in order to infer causality as a second step. From the three different geostatistical models chosen for this study (Moran's Index, SVA and experimental variogram, Fig. 4) one common picture appears: most of the density variation comes from the scales between the metre scale, that gathers all paired samples distant from 1 to 10 m and the hectometre scale, that gathers all paired samples distant from 100 to 1000 m. The Moran's Index (Fig. 4A) underlines particularly the hectometre scale where the Index decreases and crosses the zero line, changing from a distribution with almost similar densities (Moran Index above 0) to a distribution with contrasted or random densities (Moran Index value below or equal to zero, Fig. 4A). The variogram plot (Fig. 4C) confirms the preponderant role of the hectometre scale with the highest gamma value calculated. Sadly, the lack of paired samples distant from 1 m to 100 m could hide unexpected changes and prevents us from being more precise about the most significant scale. Identical limitation is visible for the SVA that equally distributes the missing variance into the scales with missing paired samples (from metre to hectometre scale). However, SVA model predicts preponderant role of at least one of these scales by the difference between the overall variance to the variance attributed to the other scales. At all events, in order to maximize information on foraminiferal density spatial distribution, we recommend designing future sampling campaigns with stations distant from 1 m to 1 km, with a particular focus on the hectometre scale.

The geostatistical models are apparently in contradiction with the importance habitats succession along salinity gradient (Debenay and Guillou, 2002) since the SVA attributes only 0.9% of the total variance to the scale of salinity changes (over 100 km), the minimum attributed to any scale. Qualitative analysis solves this discrepancy. For example, a qualitative SVA coded with values equal to 0 when no *Ammonia tepida* is observed, to 1 when *A. tepida* is a minor species (<10%) and equal to 2 when *A. tepida* is a major species (>10%) leads to drastically increase the importance of the estuarine scale (black diamonds on Fig. 4B). In the qualitative analysis, the scale over 10 km produces 41% of the total variance and therefore in strong agreement with the importance of the salinity gradient. Taken together, these results highlight the efficiency of deterministic models for qualitative predictions, understood as the order of magnitude of foraminiferal population densities and their lacks to quantify predictions. Geostatistical models represent promising tools to cross this gap especially when performed in combination with deterministic models. For example, scale analyses can by hyphened with studies of environmental processes in order to associate one preponderant process to each scale of important variation. This exercise is proposed in the following discussion.

4.2. Limiting factors at the Les Brillantes mudflat scale

The focus on Les Brillantes mudflat allows investigation of processes explaining density variations over few hundreds of meters, a critical scale identified from the geostatistic models. On one hand, our results show that the two stations present very few qualitative differences, *i.e.* changes over order of magnitudes - the most significant being *H. germanica* in September 2012 (Table 3) with high density in Station 1 probably produced by optimal conditions for development of propagules and/or reproduction during September weak riverine influence. This sensitivity tends to position *H. germanica* downstream from *A. tepida* in the estuarine succession as observed by Debenay et al. (2006) and Mojtahid et al. (2016) while Alve and Murray (1994), Debenay et al. (2000) and Debenay and Guillou (2002) observations state for the opposite. On the second hand, quantitative differences between stations are observed on every variable with 1.5–5 fold more abundance of microphytobenthos, meiofauna and macrofauna at Station 1 (Table 3) and up to 5 fold faster respiration (Table 4). The longer emersion time, hence the longer light time exposure, and the higher nutrient input, probably streaming for the grazing land of the shore via a small channel (Table 2) might favour primary production compared to Station 2 and consequently may support higher density of fauna.

The exponential relation observed between Chl a and *A. tepida* (Fig. 5A) indicates a possible deterministic relation between primary production and *A. tepida* at the hectometre scale and makes Chl a a good limiting factor for deterministic models at this scale. However, such a relation owes a lot to the opportunistic character of *A. tepida*, understood as the ability for a species to saturate rapidly the capabilities of an environment. Prolonging this interpretation, we can estimate that all parameters varying differently than Chl a have negligible effect on *A. tepida* density. Surprisingly, the co-varying parameters LI and the OPD, reputed to trace organic matter lability, evolved differently underlying the specific diet regime of *A. tepida.* Indeed, this species is known in the literature for being carnivorous (Dupuy et al., 2010), predating on metazoan classes (Chronopoulou et al., 2019) and thus may ignore variation of primary production quality. Oppositely, the literature indicates that *H. germanica* feeds mostly on diatoms notably to steal their chloroplast (Pillet et al., 2011; Cesbron et al., 2017; Jauffrais et al., 2018; LeKieffre et al., 2018). It seems that this so-called "kleptoplasty" specialisation turns into a disadvantage when facing opportunistic species in low quality high quantity food environments.

4.3. Vertical distribution of foraminifera: microhabitat vs bioturbation

4.3.1. Biomixing and chemotaxis forcing

The fine vertical sampling resolution (Fig. 3) allows a precise description of the typical exponential vertical decrease of shallow infaunal microhabitat (Buzas et al., 1993). The very shallow density maximum indicates a favourable environment, supposedly a reproduction layer and/or propagule spawning event, due to high oxygen concentration and/or fresh organic matter (Berkeley et al., 2007; de Stigter et al., 1999; Geslin et al., 2004). The progressive decrease with depth is usually associated with the biomixing produced by macrofauna bioturbation (*e.g.* Alve and Bernhard, 1995; Saffert and Thomas, 1998; Thibault de Chanvalon et al., 2015), a predation-related strategy (De Stigter et al., 1998; Loubere, 1989) or the occurrence of oxygen oases around animal burrows (Goldstein et al., 1995; Steineck and Bergstein, 1979). However, the very steep decrease of *A. tepida* (minimum reached at 0.8 cm depth) and the systematic slight re-increase at depth (except Station 2 in May 2013, Fig. 3) producing a shallow minimum density, corresponds to a specific pattern, likely produced by the combination of biomixing and chemotaxis (BC model, Thibault de Chanvalon et al., 2015). In this BC model, when buried close enough to the surface, the foraminifera detect the oxygenated layer and move back to the surface while, when buried deeper than their pseudopod length, the foraminifera are trapped at depth in a dormancy stasis, as observed by LeKieffre et al. (2017). The shallow minimum density corresponds to the chemotaxis range of the foraminifera. Oases model has been discarded in these stations because of the absence of correlation at the centimetre scale between deep living foraminifera and burrow traces (Thibault de Chanvalon et al., 2015).

In September 2012, when surface densities were high enough, *H. germanica* densities presented a similar pattern than *A. tepida* but with a less steep decrease since the shallow minimum is reached at 1.4 cm depth for *H. germanica* versus 0.6 mm for *A. tepida* (Fig. 3). On the line with the BC model, we interpret this observation as a wider chemotaxis range for *H. germanica*, maybe related to its pseudopod length, which feels necessary to move back to the surface once buried deeper than *A. tepida*. However, this difference could also come from *H. germanica* kleptoplasty, as proposed by Cesbron et al. (2017) in order to interpret similar observations. In this case, *H. germanica* would be less sensitive to

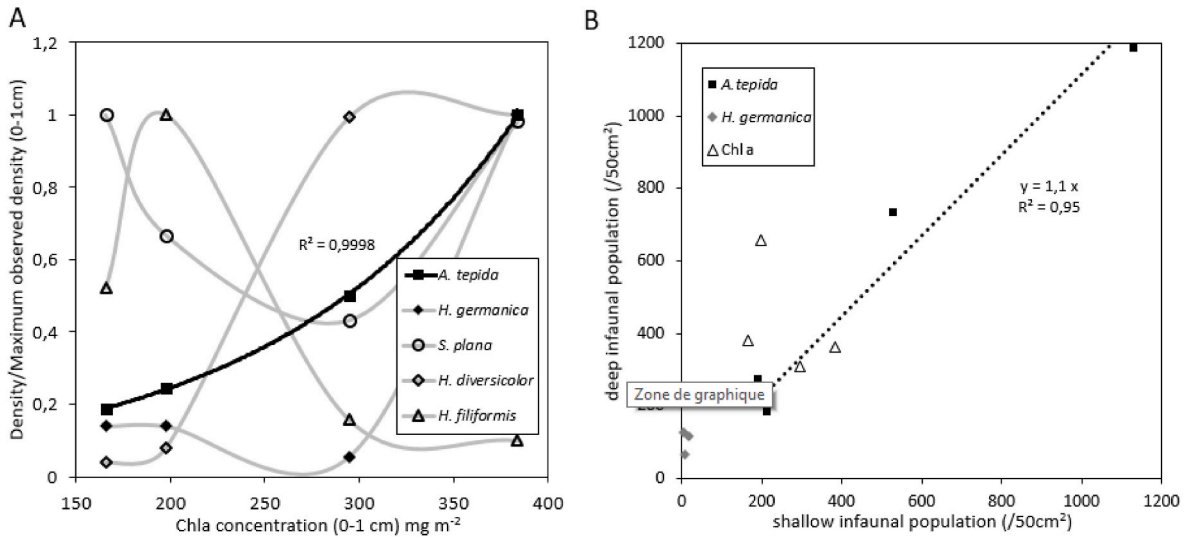

Fig. 5. A. Evolution of biological parameters in Les Brillantes according to Chl a (data from Table 2). B. Relation between deep infaunal and shallow infaunal population of *A. tepida* and *H. germanica* in Les Brillantes.

oxygen depletion and tolerates being buried deeper before moving back to the surface.

4.3.2. Deep and shallow infaunal comparison

Based on the BC model, specimens' behaviour depends on their position compared to the shallow minimum, with upper specimens being more active and especially able to reproduce and growth while lower specimens are probably in dormancy stasis. When taking into account density results from the two sampling stations in September and in May, a linear positive correlation between these two populations appears (Fig. 5B). It is a significant result as the line crosses the origin with a high R^2 value (0.95) for *A. tepida*. The relation for *H. germanica* is less convincing since the lower observed population induces higher uncertainties. However, for *A. tepida*, this relevance is highlighted by other biological parameters measured in this study such as Chl a (Fig. 5B) that does not follow any linear relation.

The model of microhabitat equilibrium (§3.6 and Fig. 2) details explicitly, despite evident oversimplifications, how the shallow and deep infaunal population interaction can be describe by their ratio, so called α, which depends of the intrinsic species dynamics (propagule spawning/reproduction and mortality rates), biomixing rate and the delay since the last change of available resources. After a certain point, function of biomixing and reproduction rate, the model shows that the time does not influence the α value anymore, slow growing species being in exponential growth while faster growing species, such as opportunists, having already saturated the environment capabilities. The constancy of the α value found for *A. tepida* ($\alpha = 1.1$, Fig. 5B) despite a 5 fold change of density indicates that during each campaign, depth repartition of foraminifera population has reached an equilibrium since the last change of available resources, more likely a saturation equilibrium. Hence biomixing is fast relatively to foraminifera resource changes. This is not the case for Chl a probably because its main resource (available light) changes too fast compared to biomixing events while foraminifera populations average short term variations of food availability. Moreover, equation (11) indicates that an α about 1 indicates high biomixing rate compared to mortality in anoxia, a first step to estimate biomixing rate using foraminifera vertical distribution. Taken together, analysis of vertical distribution confirms the steady state reached between surface resources and *A. tepida* density at surface and at depth and the importance of Chl a concentration at Les Brillantes. While the bioturbation intensity was expected to be a supplementary depth cause due to mortality increase at depth, this effect was not found to be significant since the highest density of foraminifera (including *H. germanica*) matches with the highest density of macrofauna (Fig. 5A).

5. Conclusion

Because of the several extreme conditions characterizing intertidal mudflat habitats, amongst which we can cite the risk of burial in anoxic sediments and the large daily salinity variation, the two species observed in "Les Brillantes" mudflat developed contrasting skills. *H. germanica* suffers from freshwater conditions during river flood periods but seems to get longer-range chemotaxis to face anoxia while *A. tepida* appears to be much less sensitive to freshwater inputs and favours dormancy as a strategy to overcome burial into anoxic depths. These differences could come from their different feeding strategies, *H. germanica* having a more specific diet while *A. tepida,* feeding from different sources, is emancipated from primary producer dependency and shows an opportunistic behaviour.

Geostatistic models confirm the effectiveness of average salinity to describe qualitatively the habitats distribution. However, they indicate that the density of foraminifera in these habitats are controlled by other parameters, such as Chl a, that varies over distance from 1 m to 1 km. These distances are often underrepresented in publications looking at foraminiferal heterogeneity and require supplementary investigations to state about their importance. Thus, we recommend to future models to fit geostatistical and deterministic approaches, for example, by associating a particular preponderant mechanism to each scale characterized by high heterogeneity.

Glossary

SYVEL (Surveillance system of the Loire estuary) network maintains 6 high frequency stations between Nantes and Paimboeuf for physico-chemical parameters of subsurface waters (temperature, salinity, dissolved oxygen concentration, and turbidity). Founded by the region Pays de la Loire.

SHOM is a french national military service for marine and coastal geographic information.

Banque HYDRO is a national public gathering hub of river flows, alimented mainly by numerous national services.

Declaration of competing interest

The authors report no conflict of interest.

Data availability

Data will be made available on request.

Acknowledgement

This study is part of the RS2E–OSUNA project funded by the Région Pays de la Loire and benefits from the campaign Halioloire 1 (10.17600/12120050). The authors want to thank the associate editor and reviewers for their valuable suggestions to improve this manuscript. Thanks also to E. Cheveau, E. Beneteau, A. Mouret, for their help during sampling and picking.

12 Appendices

12.1 Appendix 1: Demonstration that the variance of a dataset hierarchized over k scale is equal to the sum of the mean scale variance of each scale

Based on the definition of the variance and on the formalism previously described, samples' value are the x_i^1 (they belong to the scale 1) and the global mean is x^k, we have:

$$VAR = V^{1\to k} = \frac{1}{N^1}\sum_{i=1}^{N^1}\left(x_i^1 - x^k\right)^2 \tag{A1}$$

$$V^{1\to k} = \frac{1}{N^1}\left(\sum_{i=1}^{N^1}\left(x_i^1\right)^2 - N^1\left(x^k\right)^2\right) \tag{A2}$$

The samples can be gathered in n^{k-1} group whose extension belong to the scale k-1. There is N^1/n^{k-1} samples per group and the x_j^{k-1} are the means of each groups and the x_i^1 are now written as x_{ij}^1, with the subscript j indicates to which groups the sample belong.

$$V^{1\to k} = \frac{1}{N^1}\left(\sum_{i=1}^{N^1}\left(x_{i,j}^1\right)^2 - \sum_{j=1}^{n^{k-1}}\frac{N^1}{n^{k-1}}\left(x_j^{k-1}\right)^2 + \sum_{j=1}^{n^{k-1}}\frac{N^1}{n^{k-1}}\left(x_j^{k-1}\right)^2 - N^1\left(x^k\right)^2\right)$$

$$V^{1\to k} = \frac{1}{N^1}\sum_{j=1}^{n^{k-1}}\left(\sum_{i=1}^{\frac{N^1}{n^{k-1}}}\left(x_{i,j}^1\right)^2 - \frac{N^1}{n^{k-1}}\left(x_j^{k-1}\right)^2\right) + \frac{1}{n^{k-1}}\left(\sum_{j=1}^{n^{k-1}}\left(x_j^{k-1}\right)^2 - n^{k-1}\left(x^k\right)^2\right)$$

$$V^{1\to k} = \frac{1}{N^1}\sum_{j=1}^{n^{k-1}}\frac{N^1}{n^{k-1}}V_j^{1\to k-1} + V^{k-1\to k}$$

$$V^{1\to k} = \frac{1}{n^{k-1}}\sum_{j=1}^{n^{k-1}}V_j^{1\to k-1} + V^{k-1\to k} \tag{A3}$$

The property expressed by A3 is true also for any j and p, $V_j^{1\to k-p}$, especially

$$V_j^{1\to k-1} = \frac{1}{n^{k-2}}\sum_{l=1}^{n^{k-2}}V_{j,l}^{1\to k-2} + V_j^{k-2\to k-1} \tag{A4}$$

Once you inject A4 into A3 you get,

$$V^{1\to k} = \frac{1}{n^{k-1}}\frac{1}{n^{k-2}}\sum_{j=1}^{n^{k-1}}\sum_{l=1}^{n^{k-2}}V_{j,l}^{1\to k-2} + \frac{1}{n^{k-1}}\sum_{j=1}^{n^{k-1}}V_j^{k-2\to k-1} + V^{k-1\to k} \tag{A5}$$

Then using the property expressed by A3 for p = 2 you get

$$V^{1\to k} = \frac{1}{n^{k-1}}\frac{1}{n^{k-2}}\frac{1}{n^{k-3}}\sum_{j=1}^{n^{k-1}}\sum_{l=1}^{n^{k-2}}\sum_{m=1}^{n^{k-3}}V_{j,l,m}^{1\to k-3} + \frac{1}{n^{k-1}}\frac{1}{n^{k-2}}\sum_{j=1}^{n^{k-1}}\sum_{l=1}^{n^{k-2}}V_{j,l}^{k-3\to k-2} + \frac{1}{n^{k-1}}\sum_{j=1}^{n^{k-1}}V_j^{k-2\to k-1} + V^{k-1\to k} \tag{A6}$$

Repeating this for all p until p = k-2

$$V^{1\to k} = \frac{1}{N^2}\sum_{j=1}^{n^{k-1}}V_j^{1\to 2} + \ldots + \frac{1}{N^{k-2}}\sum_{j=1}^{N^{k-2}}V_j^{k-3\to k-2} + \frac{1}{N^{k-1}}\sum_{j=1}^{N^{k-1}}V_j^{k-2\to k-1} + V^{k-1\to k} \tag{A7}$$

$$VAR = V^{1\to k} = \sum_{h=1}^{k-1}\overline{V^{h\to h+1}}$$

12.2 Appendix 2: Demonstration of the expression of the mean of the scale variance as a function of the relative scale variance

Based on the relative scale variance definition, for any i:

$$RV^{h\to h+1} = \frac{1}{\left(x^{h+1}\right)^2}\left(\frac{1}{n^h}\sum_{i=1}^{n^h}\left(x_i^h\right)^2 - \left(x^{h+1}\right)^2\right) \tag{B1}$$

Once reorganized, we get:

$$\sum_{i=1}^{n^h}\left(x_i^h\right)^2 = \left(1+RV^{h\to h+1}\right)n^h\left(x^{h+1}\right)^2$$

By sum over all the j group from the scale h+1,

$$\sum_{j=1}^{N^{h+1}}\sum_{i=1}^{n^h}\left(x_i^h\right)^2 = \sum_{j=1}^{N^{h+1}}\left(1+RV^{h\to h+1}\right)n^h\left(x^{h+1}\right)^2$$

$$\sum_{i=1}^{N^h}\left(x_i^h\right)^2 = \left(1+RV^{h\to h+1}\right)n^h\sum_{j=1}^{N^{h+1}}\left(x_j^{h+1}\right)^2 \tag{B2}$$

equation (B2) express the sum of the square at the scale h, as a function of the sum of the square at the scale h+1. Injecting p times equation (B2) into itself, we get:

$$\sum_{i=1}^{N^h}\left(x_i^h\right)^2 = \prod_{i=h}^{h+p-1}\left(1+RV^{i\to i+1}\right)n^i\sum_{j=1}^{N^{h+p}}\left(x_j^{h+p}\right)^2 \tag{B3}$$

On another hand, taking the definition of the mean scale variance, we have:

$$\overline{V^{h\to h+1}} = \frac{1}{N^{h+1}}\sum_{i=1}^{N^{h+1}}\left(x_i^{h+1}\right)^2 RV^{h\to h+1} \tag{B4}$$

Injecting B3 into B4, with p = k-1-h,

$$\overline{V^{h\to h+1}} = \frac{RV^{h\to h+1}}{N^{h+1}}\prod_{i=h+1}^{k-1}\left(1+RV^{i\to i+1}\right)n^i\sum_{j=1}^{N^k}\left(x_j^k\right)^2$$

$$\overline{V^{h\to h+1}} = \frac{RV^{h\to h+1}}{N^k}\prod_{i=h+1}^{k-1}\left(1+RV^{i\to i+1}\right)\sum_{j=1}^{N^k}\left(x_j^k\right)^2 \tag{B5}$$

References

Alve, E., 1999. Colonization of new habitats by benthic foraminifera: a review. Earth Sci. Rev. 46, 167–185. https://doi.org/10.1016/S0012-8252(99)00016-1.

Alve, E., Bernhard, J.M., 1995. Vertical migratory response of benthic foraminifera to controlled oxygen concentrations in an experimental mesocosm. Mar. Ecol. Prog. Ser. 116, 137–151. https://doi.org/10.3354/meps116137.

Alve, E., Murray, J.W., 2001. Temporal variability in vertical distributions of live (stained) intertidal foraminifera, Southern England. J. Foraminifer. Res. 31, 12–24. https://doi.org/10.2113/0310012.

Alve, E., Murray, J. w, 1994. Ecology and taphonomy of benthic foraminifera in a temperate mesotidal inlet. J. Foraminifer. Res. 24, 18–27. https://doi.org/10.2113/gsjfr.24.1.18.

Benyoucef, I., 2014. Télédétection visible proche-infrarouge de la distribution spatio-temporelle du microphytobenthos estuarien (Ph.D. thesis). Université de Nantes.

Berg, P., Risgaard-Petersen, N., Rysgaard, S., 1998. Interpretation of measured concentration profiles in sediment pore water. Limnol. Oceanogr. 43, 1500–1510. https://doi.org/10.4319/lo.1998.43.7.1500.

Berkeley, A., Perry, C.T., Smithers, S.G., Horton, B.P., 2008. The spatial and vertical distribution of living (stained) benthic foraminifera from a tropical, intertidal environment, north Queensland, Australia. Mar. Micropaleontol. 69, 240–261. https://doi.org/10.1016/j.marmicro.2008.08.002.

Berkeley, A., Perry, C.T., Smithers, S.G., Horton, B.P., Taylor, K.G., 2007. A review of the ecological and taphonomic controls on foraminiferal assemblage development in intertidal environments. Earth Sci. Rev. 83, 205–230. https://doi.org/10.1016/j.earscirev.2007.04.003.

Bernhard, J.M., Ostermann, D.R., Williams, D.S., Blanks, J.K., 2006. Comparison of two methods to identify live benthic foraminifera: A test between Rose Bengal and CellTracker Green with implications for stable isotope paleoreconstructions. Paleoceanography 21, PA4210. https://doi.org/10.1029/2006PA001290.

Bianchi, T.S., Findlay, S., 1991. Decomposition of hudson estuary macrophytes: photosynthetic pigment transformations and decay constants. Estuaries 14, 65. https://doi.org/10.2307/1351983.

Bird, C., Schweizer, M., Roberts, A., Austin, W.E.N., Knudsen, K.L., Evans, K.M., Filipsson, H.L., Sayer, M.D.J., Geslin, E., Darling, K.F., 2020. The genetic diversity, morphology, biogeography, and taxonomic designations of Ammonia (Foraminifera) in the Northeast Atlantic. Mar. Micropaleontol. 155, 101726. https://doi.org/10.1016/j.marmicro.2019.02.001.

Bivand, R.S., Wong, D.W.S., 2018. Comparing implementations of global and local indicators of spatial association. Test 27, 716–748. https://doi.org/10.1007/s11749-018-0599-x.

Bradshaw, J.S., 1961. Laboratory experiments on the ecology of foraminifera. Cushman Found Foram Res Contr 12, 87–106.

Buzas, M.A., Culver, S.J., Jorissen, F.J., 1993. A statistical evaluation of the microhabitats of living (stained) infaunal benthic foraminifera. Mar. Micropaleontol. 20, 311–320. https://doi.org/10.1016/0377-8398(93)90040-5.

Cartaxana, P., Jesus, B., Brotas, V., 2003. Pheophorbide and pheophytin a-like pigments as useful markers for intertidal microphytobenthos grazing by Hydrobia ulvae. Estuar. Coast Shelf Sci. 58, 293–297. https://doi.org/10.1016/S0272-7714(03)00081-7.

Cesbron, F., Geslin, E., Jorissen, F.J., Delgard, M.L., Charrieau, L., Deflandre, B., Jézéquel, D., Anschutz, P., Metzger, E., 2016. Vertical distribution and respiration rates of benthic foraminifera: Contribution to aerobic remineralization in intertidal mudflats covered by Zostera noltei meadows. Estuar. Coast Shelf Sci. 179, 23–38. https://doi.org/10.1016/j.ecss.2015.12.005. Special Issue: Functioning and dysfunctioning of Marine and Brackish Ecosystems.

Cesbron, F., Geslin, E., Kieffre, C.L., Jauffrais, T., Nardelli, M.P., Langlet, D., Mabilleau, G., Jorissen, F.J., Jézéquel, D., Metzger, E., 2017. Sequestered chloroplasts in the benthic foraminifer haynesina germanica: cellular organization, oxygen fluxes and potential ecological implications. J. Foraminifer. Res. 47, 268–278. https://doi.org/10.2113/gsjfr.47.3.268.

Chronopoulou, P.-M., Salonen, I., Bird, C., Reichart, G.-J., Koho, K.A., 2019. Metabarcoding insights into the trophic behavior and identity of intertidal benthic foraminifera. Front. Microbiol. 10 https://doi.org/10.3389/fmicb.2019.01169.

Coynel, A., Gorse, L., Curti, C., Schafer, J., Grosbois, C., Morelli, G., Ducassou, E., Blanc, G., Maillet, G.M., Mojtahid, M., 2016. Spatial distribution of trace elements in the surface sediments of a major European estuary (Loire Estuary, France): Source

identification and evaluation of anthropogenic contribution. J. Sea Res. 118, 77–91. https://doi.org/10.1016/j.seares.2016.08.005.
De Stigter, H., Jorissen, F., Van der Zwaan, G., 1998. Bathymetric distribution and microhabitat partitioning of live (Rose Bengal stained) benthic foraminifera along a shelf to bathyal transect in the southern Adriatic Sea. J. Foraminifer. Res. 28, 40–65.
de Stigter, H.C., van der Zwaan, G.J., Langone, L., 1999. Differential rates of benthic foraminiferal test production in surface and subsurface sediment habitats in the southern Adriatic Sea. Palaeogeogr. Palaeoclimatol. Palaeoecol. 149, 67–88. https://doi.org/10.1016/S0031-0182(98)00193-X.
Debenay, J.-P., Bicchi, E., Goubert, E., Armynot du Châtelet, E., 2006. Spatio-temporal distribution of benthic foraminifera in relation to estuarine dynamics (Vie estuary, Vendée, W France). Estuar. Coast Shelf Sci. 67, 181–197. https://doi.org/10.1016/j.ecss.2005.11.014.
Debenay, J.-P., Guillou, J.-J., 2002. Ecological transitions indicated by foraminiferal assemblages in paralic environments. Estuaries 25, 1107–1120. https://doi.org/10.1007/BF02692208.
Debenay, J.-P., Guillou, J.-J., Redois, F., Geslin, E., 2000. Distribution trends of foraminiferal assemblages in paralic environments. In: Martin, R.E. (Ed.), Environmental Micropaleontology. Springer US, pp. 39–67.
Debenay, J.-P., Guillou, J.-J., Tsakiridis, E., de Casamajor, M.-N., 2001. Bioindicateurs d'impact dans les ports et les estuaires: les foraminifères. Rev. Fr. Génie Civ. 5, 1105–1122.
Dupuy, C., Rossignol, L., Geslin, E., Pascal, P.-Y., 2010. Predation of mudflat meio-macrofaunal metazoans by a calcareous foraminifer, Ammonia tepida (cushman, 1926). J. Foraminifer. Res. 40, 305–312. https://doi.org/10.2113/gsjfr.40.4.305.
Fortin, M.-J., Dale, M.R.T., 2005. Spatial Analysis a Guide for Ecologists. Cambridge University Press, Cambridge, N.Y.
Geslin, E., Heinz, P., Jorissen, F., Hemleben, Ch, 2004. Migratory responses of deep-sea benthic foraminifera to variable oxygen conditions: laboratory investigations. Mar. Micropaleontol. 53, 227–243. https://doi.org/10.1016/j.marmicro.2004.05.010.
Geslin, E., Risgaard-Petersen, N., Lombard, F., Metzger, E., Langlet, D., Jorissen, F., 2011. Oxygen respiration rates of benthic foraminifera as measured with oxygen microsensors. J. Exp. Mar. Biol. Ecol. 396, 108–114. https://doi.org/10.1016/j.jembe.2010.10.011.
Goldstein, S.T., Watkins, G.T., Kuhn, R.M., 1995. Microhabitats of salt marsh foraminifera: st. Catherines island, Georgia, USA. Mar. Micropaleontol., selected papers from the fifth. International Symposium of Foraminifera 26, 17–29. https://doi.org/10.1016/0377-8398(95)00006-2.
Hohenegger, J., Piller, W.E., Baal, C., 1993. Horizontal and vertical spatial microdistribution of foraminifers in the shallow subtidal Gulf of Trieste, northern Adriatic Sea. J. Foraminifer. Res. 23, 79–101. https://doi.org/10.2113/gsjfr.23.2.79.
Jauffrais, T., LeKieffre, C., Koho, K.A., Tsuchiya, M., Schweizer, M., Bernhard, J.M., Meibom, A., Geslin, E., 2018. Ultrastructure and distribution of kleptoplasts in benthic foraminifera from shallow-water (photic) habitats. Mar. Micropaleontol., Benthic Foraminiferal Ultrastructure Studies 138, 46–62. https://doi.org/10.1016/j.marmicro.2017.10.003.
Jorissen, F.J., de Stigter, H.C., Widmark, J.G.V., 1995. A conceptual model explaining benthic foraminiferal microhabitats. Mar. Micropaleontol. 26, 3–15. https://doi.org/10.1016/0377-8398(95)00047-X.
Kitazato, H., Shirayama, Y., Nakatsuka, T., Fujiwara, S., Shimanaga, M., Kato, Y., Okada, Y., Kanda, J., Yamaoka, A., Masuzawa, T., Suzuki, K., 2000. Seasonal phytodetritus deposition and responses of bathyal benthic foraminiferal populations in Sagami Bay, Japan: preliminary results from [a]Project Sagami 1996±1999[o]. Mar. Micropaleontol. 15.
Langlet, D., Baal, C., Geslin, E., Metzger, E., Zuschin, M., Riedel, B., Risgaard-Petersen, N., Stachowitsch, M., Jorissen, F.J., 2014. Foraminiferal species responses to in situ, experimentally induced anoxia in the Adriatic Sea. Biogeosciences 11, 1775–1797. https://doi.org/10.5194/bg-11-1775-2014.
Le Floch, J.-F, 1961. Propagation de la marée dynamique dans l'estuaire de la Seine et en Seine maritime. (Thèse). Paris. In: Moran, P.A. (Ed.), 1950. Notes on continuous stochastic phenomena. Biometrika 37, pp. 17–23.
Legendre, P., Fortin, M.-J., 1989. Spatial pattern and ecological analysis. Vegetatio 80, 107–138.
LeKieffre, C., Jauffrais, T., Geslin, E., Jesus, B., Bernhard, J.M., Giovani, M.-E., Meibom, A., 2018. Inorganic carbon and nitrogen assimilation in cellular compartments of a benthic kleptoplastic foraminifer. Sci. Rep. 8, 1–12. https://doi.org/10.1038/s41598-018-28455-1.
LeKieffre, C., Spangenberg, J.E., Mabilleau, G., Escrig, S., Meibom, A., Geslin, E., 2017. Surviving anoxia in marine sediments: the metabolic response of ubiquitous benthic foraminifera (Ammonia tepida). PLoS One 12, e0177604.
Levin, S.A., 1976. Population dynamic models in heterogeneous environments. Annu. Rev. Ecol. Systemat. 287–310.
Loubere, P., 1989. Bioturbation and sedimentation rate control of benthic microfossil taxon abundances in surface sediments: a theoretical approach to the analysis of species microhabitats. Mar. Micropaleontol. 14, 317–325. https://doi.org/10.1016/0377-8398(89)90016-9.
Méléder, V., Barillé, L., Rincé, Y., Morançais, M., Rosa, P., Gaudin, P., 2005. Spatio-temporal changes in microphytobenthos structure analysed by pigment composition in a macrotidal flat (Bourgneuf Bay, France). Mar. Ecol. Prog. Ser. 297, 83–99. https://doi.org/10.3354/meps297083.
Moellering, H., Tobler, W., 1972. Geographical variances. Geogr. Anal. 4, 34–50. https://doi.org/10.1111/j.1538-4632.1972.tb00455.x.
Mojtahid, M., Geslin, E., Coynel, A., Gorse, L., Vella, C., Davranche, A., Zozzolo, L., Blanchet, L., Bénéteau, E., Maillet, G., 2016. Spatial distribution of living (Rose Bengal stained) benthic foraminifera in the Loire estuary (western France). J. Sea Res. https://doi.org/10.1016/j.seares.2016.02.003.
Murray, J.W., 2006. Ecology and Applications of Benthic Foraminifera. Cambridge University Press, Cambridge.
Pillet, L., de Vargas, C., Pawlowski, J., 2011. Molecular identification of sequestered diatom chloroplasts and kleptoplastidy in foraminifera. Protist 162, 394–404. https://doi.org/10.1016/j.protis.2010.10.001.
Richirt, J., Schweizer, M., Bouchet, V.M.P., Mouret, A., Quinchard, S., Jorissen, F.J., 2019. Morphological distinction of three Ammonia phylotypes occurring along European coasts. J. Foraminifer. Res. 49, 76–93. https://doi.org/10.2113/gsjfr.49.1.76.
Saffert, H., Thomas, E., 1998. Living foraminifera and total populations in salt marsh peat cores: kelsey Marsh (Clinton, CT) and the Great Marshes (Barnstable, MA). Mar. Micropaleontol. 33, 175–202. https://doi.org/10.1016/S0377-8398(97)00035-2.
Schönfeld, J., Alve, E., Geslin, E., Jorissen, F., Korsun, S., Spezzaferri, S., 2012. The FOBIMO (FOraminiferal BIo-MOnitoring) initiative—towards a standardised protocol for soft-bottom benthic foraminiferal monitoring studies. Mar. Micropaleontol. 94–95, 1–13. https://doi.org/10.1016/j.marmicro.2012.06.001.
Steineck, P.L., Bergstein, J., 1979. Foraminifera from hommocks salt-marsh, Larchmont harbor, New York. J. Foraminifer. Res. 9, 147–158.
Talley, T.S., 2007. Which spatial heterogeneity framework? Consequences for conclusions about patchy population distributions. Ecology 88, 1476–1489.
Thibault de Chanvalon, A., Metzger, E., Mouret, A., Cesbron, F., Knoery, J., Rozuel, E., Launeau, P., Nardelli, M.P., Jorissen, F.J., Geslin, E., 2015. Two-dimensional distribution of living benthic foraminifera in anoxic sediment layers of an estuarine mudflat (Loire estuary, France). Biogeosciences 12, 6219–6234. https://doi.org/10.5194/bg-12-6219-2015.
Thibault de Chanvalon, A., Mouret, A., Knoery, J., Geslin, E., Péron, O., Metzger, E., 2016. Manganese, iron and phosphorus cycling in an estuarine mudflat, Loire, France. J. Sea Res. 118, 92–102. https://doi.org/10.1016/j.seares.2016.10.004.
Weinmann, A.E., Goldstein, S.T., 2017. Landward-directed Dispersal of Benthic Foraminiferal Propagules At Two Shallow-water Sites in the Doboy Sound Area (Georgia, U.S.A.). J. Foraminifer. Res. 47, 325–336. https://doi.org/10.2113/gsjfr.47.4.325.
Wu, J., Jelinski, D.E., Luck, M., Tueller, P.T., 2000. Multiscale Analysis of Landscape Heterogeneity: Scale Variance and Pattern Metrics. Geo Inf. Sci. 6, 6–19. https://doi.org/10.1080/10824000009480529.